Photocatalysis

Deutsche Ausgabe: DOI: 10.1002/ange.201511580
Internationale Ausgabe: DOI: 10.1002/anie.201511580

TiO_2 Nanotubes: Nitrogen-Ion Implantation at Low Dose Provides Noble-Metal-Free Photocatalytic H_2-Evolution Activity

*Xuemei Zhou, Volker Häublein, Ning Liu, Nhat Truong Nguyen, Eva M. Zolnhofer, Hiroaki Tsuchiya, Manuela S. Killian, Karsten Meyer, Lothar Frey, and Patrik Schmuki**

Abstract: *Low-dose nitrogen implantation induces an ion and damage profile in TiO_2 nanotubes that leads to "co-catalytic" activity for photocatalytic H_2-evolution (without the use of any noble metal). Ion implantation with adequate parameters creates this active zone limited to the top part of the tubes. The coupling of this top layer and the underlying non-implanted part of the nanotubes additionally contributes to an efficient carrier separation and thus to a significantly enhanced H_2 generation.*

Ever since the groundbreaking work of Fujishima and Honda[1] in 1972, photocatalytic water splitting has attracted tremendous research interest. The process is the application of a simple photoelectrochemical principle: If light (preferably solar light) is irradiated on a semiconductor, electron–hole pairs are generated that may react at the semiconductor surface with redox couples in the surroundings (if the energetic positions of conduction and valence band relative to the corresponding redox potentials are suitable).[2] In spite of hundreds of investigations on a wide range of photocatalysts, TiO_2 still remains the most investigated semiconductive material for photocatalytic hydrogen generation from various electrolytes (with or without sacrificial agents), as it has a conduction band-edge level compatible with the generation of H_2 from water, is economically and ecologically sound, and especially as it has a very high (photo)corrosion resistance.[2,3]

Nevertheless, a main setback of using titania is that the charge-transfer reaction kinetics on plain TiO_2 surfaces and thus the H_2 production rates are extremely slow if no co-catalysts such as Pt, Pd, or Au are being used.[4,5] These noble-metal co-catalysts facilitate or stimulate the transfer of photogenerated electrons from the conduction band to the surrounding and thus promote hydrogen production.[6] The use of such a noble-metal co-catalyst, however, puts into question the economic benefit of using cost-friendly TiO_2 as a base material.

Therefore pathways to create noble-metal-free hydrogen-evolution activity on TiO_2 are not only of considerable scientific but also of high economic interest. Up to now few studies investigated the formation of an intrinsically increased reactivity of titania for H_2 generation.[7] Nevertheless, for a number of photocatalytic reactions, various defects in TiO_2 surfaces are recognized to strongly affect photocatalytic rates but are also known to be unstable if not present in a sub-surface configuration.[8]

A most efficient way to introduce sub-surface lattice defects (namely vacancy/interstitial pairs) into any crystalline material is high energy ion implantation.[9]

Herein we introduce the use of low levels of nitrogen-ion implantation into TiO_2 nanotube layers to modify them with a defined ion and defect distribution. These nanotubes (NTs) then are investigated for their photocatalytic H_2 generation under solar light illumination. The results show that N-implantation (and the accompanied lattice damage), at sufficiently low dose, can effectively induce an activation of anatase TiO_2 NTs for noble-metal-free photocatalytic H_2 evolution (Figure 1).

We selected nitrogen ions for implantation, not only because they allow the creation of highly controllable lattice damage but also as they are expected to potentially provide additional beneficial effects regarding the electronic properties of the TiO_2 NTs.[10,11]

For our experiments we used self-organized TiO_2 nanotube layers grown from titanium metal sheets by electrochemical anodization in an NH_4F/H_2O/EG electrolyte. Such layers are shown in Figure 1 a and consist of individual tubes of 80 nm in diameter and a length of 6 μm. Alternatively some tube layers were grown to a length of approximately 500 nm (more details are given in the Supporting Information). The NT-layers were then converted by air annealing at 450 °C to an anatase structure (as anatase is the most efficient polymorph of TiO_2 for photocatalytic H_2 generation[7b,8a]). For reference purposes also non annealed, that is, amorphous TiO_2 NTs were investigated (see Figure S9–11 in the Supporting Information).

Ion implantation was carried out with a Varian 350 D ion implanter at 60 keV at doses of 8×10^{14} ions cm^{-2} and $1\times$

[*] X. Zhou, Dr. N. Liu, N. T. Nguyen, Dr. M. S. Killian, Prof. Dr. P. Schmuki
Department of Materials Science WW-4, LKO
University of Erlangen-Nuremberg
Martensstrasse 7, 91058 Erlangen (Germany)
E-mail: schmuki@ww.uni-erlangen.de
Dr. V. Häublein, Prof. Dr. L. Frey
Fraunhofer Institute for Integrated Systems and Device Technology IISB, Schottkystrasse 10, 91058 Erlangen (Germany)
E. M. Zolnhofer, Prof. Dr. K. Meyer
Department of Chemistry and Pharmacy, Inorganic Chemistry
Friedrich-Alexander University Erlangen-Nürnberg (FAU)
Egerlandstrasse 1, 91058 Erlangen (Germany)
Dr. H. Tsuchiya
Division of Materials and Manufacturing Science
Graduate School of Engineering, Osaka University
2-1 Yamada-oka, Suita, Osaka 565–0871 (Japan)

Supporting information (sample preparation, additional characterization and further discussion of the results) for this article can be found under http://dx.doi.org/10.1002/anie.201511580.

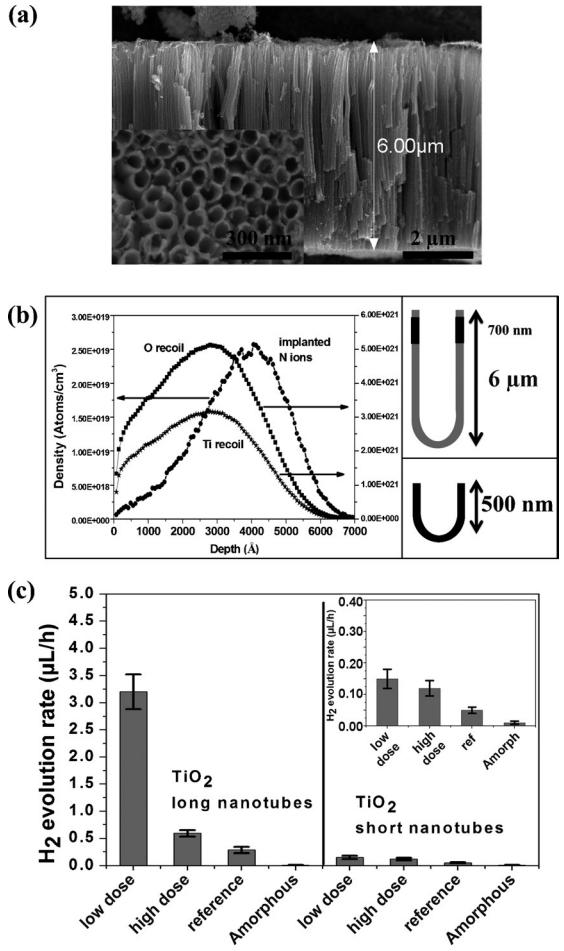

Figure 1. a) SEM images of TiO_2 nanotube layers (ca. 6 µm long) in cross-section and top view (inset). b) SRIM simulation of depth-distribution of N ions and damage (Ti recoil and O recoil) in a TiO_2 nanotube target with an energy of 60 keV at a dose of 8×10^{14} atoms cm^{-2}. Right: schematic illustration of the damage (black) to tubes of different lengths. c) Photocatalytic H_2 evolution from TiO_2-NTs long (6 µm, Figure 1a) and short (500 nm, Figure S3) under AM 1.5 (100 mW cm^{-2}). For the nitrogen implant, two doses of 8×10^{14} ions cm^{-2} (low dose) and 1×10^{16} ions cm^{-2} (high dose) are shown, along with results for non-implanted reference (annealed) and amorphous (non-annealed) TiO_2 nanotube layers.

10^{16} ions cm^{-2}, respectively. Figure 1b shows the results of SRIM simulations[9] of the depth distributions for implanted nitrogen ions, as well as damage (by oxygen recoil and titanium recoil). The simulations show, at 60 keV implantation, a maximum for the nitrogen ion implant located at approximately 200–600 nm below the surface and a maximum in point defect damage at around 100–500 nm below the surface. To verify the implant profile and presence of N, we carried out a GDOES depth profile for nitrogen as described in the Supporting Information, Figure S7 as well as XPS and TOF-SIMS measurements (Figure S5, S6, S7 and discussion).

Note (c.f. GDOES profile and simulations) that for the shorter tubes (500 nm), the implant/damage profile penetrates the full tube length, whereas for the longer tubes (6 µm) ion implantation leads to a modification only in the top part of the tubes (illustrated in Figure 1b and discussed in more detail in the Supporting Information). Figure 1c shows that ion implantation can have a strong effect on the photocatalytic H_2 production rate. Interestingly the tube layers that were exposed to a low-N-dose show a strongly enhanced activity, while the tubes implanted with a higher dose show virtually no or only a small effect. Moreover, the beneficial effect of low-dose nitrogen implantation is much more pronounced for the longer TiO_2-NTs than for the short tubes (although both contain the same ion- and damage doses and distributions). This strongly suggests that photogenerated electrons in the intact part of the long tubes can reach the implanted zone and react there to form H_2.

To characterize the effects of N-implantation on the structure of the NTs, we studied the layers before and after nitrogen implantation by XRD, Raman spectroscopy, and TEM. From XRD taken for a tube layer as shown in Figure 1a, a clear decrease of the anatase main peak located at 25.2° can be seen after high-dose N implantation (Figure 2a). This is in line with a partial amorphization of the tubes after implantation (see also XRD for amorphous TiO_2 NTs).[12] For the low-dose nitrogen implantation, no apparent decrease of the anatase peak or broadening is evident from XRD spectra. From Raman spectra (Figure 2b) for plain TiO_2 NTs a typical anatase Raman signature can be obtained. The high-dose implanted TiO_2 NTs show a significant decrease of the signals in line with amorphization.[13] For the low-dose implant NTs, however, the peak intensity of all modes (Figure 2b inset) decreases only slightly without a clear change in the position of the Raman band. Such an effect in Raman spectra has been reported for the introduction of point defects in TiO_2 (e.g. by the presence of an increased vacancy concentration[5b,14]).

Based on the SRIM simulation and the GDOES profile (Figure 1b, Figure S1, S7), the damage and implant concentration reaches a maximum at 200–600 nm below the surface. Therefore we studied the tubes at various depths with HRTEM and corresponding SAED. Figure 2c shows SAED patterns taken at different distances from the tube top for a 6 µm long nanotube. Even if the tube is implanted at a higher dose (1×10^{16} ions cm^{-2}), in the upmost zone the SAED image reveals a clear anatase signature. However, for SAED taken in the range of 400 nm to 600 nm below the top, the patterns reveal almost total amorphization of the tube walls. This amorphization in the maximum-damage zone of high-dose nitrogen implantation is also visible from HRTEM images (see Figure S4). In contrast, for samples implanted at a lower dose even in the maximum damage zone, no changes in the reflex-patterns or blurring in the SAED is apparent—that is, a clear anatase pattern is obtained. This indicates that under these conditions the introduced damage is not sufficient to significantly alter the basic anatase character of the tube wall. SAED for tube regions at 1.5 µm below the top and lower shows again clear patterns of crystalline anatase for both implant doses.

To characterize the tubes in view of a modification of the electronic and electrochemical properties we carried out impedance and photoelectrochemical measurements as shown in Figure 3 and discussed in detail in the Supporting Information, Figure S8. Additionally we investigated the

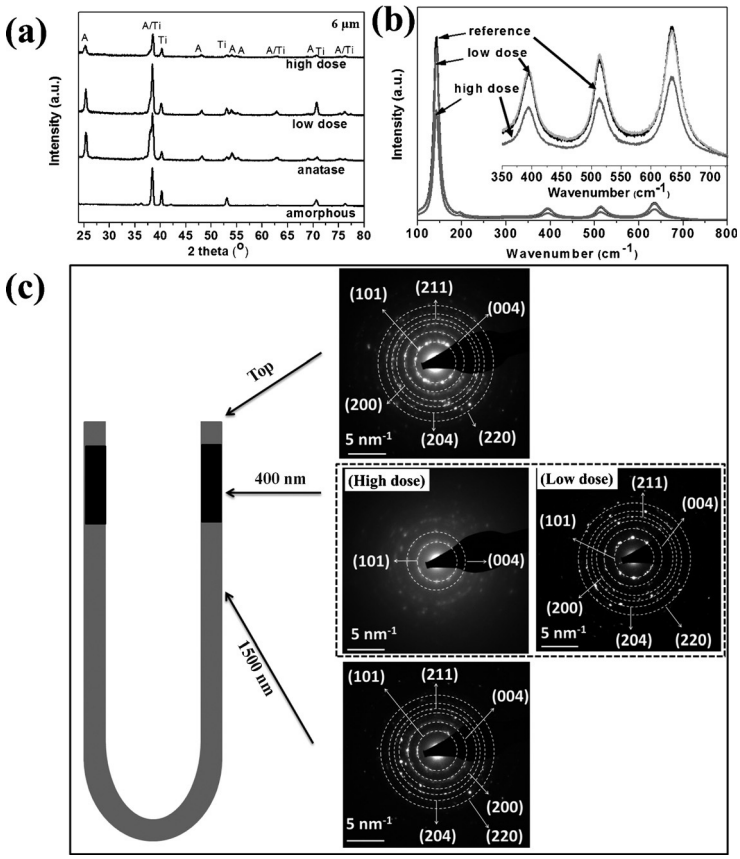

Figure 2. a) X-ray diffraction (XRD) and b) Raman spectra of TiO_2 nanotube layers (as shown in Figure 1 a) before and after N implantation with doses of 8×10^{14} ions cm^{-2} and 1×10^{16} ions cm^{-2}, c) SAED patterns of N-implanted TiO_2 NTs with a high dose of 1×10^{16} ions cm^{-2}, taken at the top, at 400 nm to 600 nm below the surface, and at 1500 nm below the surface showing amorphization in the maximum implant zone (100–500 nm below the surface). Right image: SAED at same level (400 nm to 600 nm) below surface for low dose (8×10^{14} ions cm^{-2}) implantation showing a still-intact anatase pattern.

effects induced by ion implantation by solid state *I–V* curves as shown and discussed in Figure S9.

Overall, the results of Figure 3 a–d show that nitrogen implantation generally increases the doping concentration, and the high dose has detrimental effects on the photocurrent magnitude, leads to excessive charge carrier recombination and a high charge-carrier-transfer resistance to the electrolyte. These effects, to a large extent, can be ascribed to amorphization of the anatase structure by ion-beam damage that strongly affects the tubes detrimentally in view of electrical (Figure S10) and photoelectrochemical properties (Figure S11). Low dose N implantation, on the other hand, leads to an increase of the sub-band-gap response in anatase (states ca. 0.2 eV below the conduction band) that drastically reduces the charge-transfer resistance (see Supporting Information).

For the longer tubes, low-dose ion implantation leads thus to an active zone close to the tube top that provides beneficial co-catalytic and electronic effects. In this case, additionally, photogenerated electrons from underlying intact parts of the tube can reach this active zone. (This seems plausible considering that light with an energy in the band-gap region of anatase has an absorption depth into TiO_2 nanotubes of a few μm and that anatase tubes provide an electron diffusion length in the range of several 10 μm.[3b,15])

Thus an electron harvesting/charge-transfer-activity combination is established that significantly contributes to the overall H_2 evolution efficiency. Electron transfer towards the implanted zone may further be facilitated by the fact that a beneficial electronic junction is formed (as illustrated in Figure S12).

To gain additional information on the nature of the defects induced by low-dose ion implantation we used electron paramagnetic resonance spectroscopy (EPR).[16] Figure 4 a shows the CW X-band EPR spectra for the reference, the low- and the high-dose nitrogen-implanted TiO_2 nanotubes recorded at a temperature of 7 K (liquid He). In the spectrum of the plain TiO_2 NTs, only trace amounts of defects ("F-centers" or oxygen vacancies[17]) are detectable. For the implanted samples, an additional and significantly stronger signal is apparent.[11b] Interpretation of the EPR spectra (Figure S13 and discussion) suggests that this signature can be attributed to a combination of Ti^{3+}/N_b (N_b: bulk nitrogen in substitutional or interstitial position). This configuration stabilizes Ti^{3+} centers by charge-transfer resonance (Figure S14)[11] and thus, such Ti^{3+} species are regarded as particularly robust against re-oxidation.

The higher dose implant exhibits the same characteristic EPR spectrum but with a higher signal intensity. In other words, also in the high-dose-implant material the same type of defect pattern is present but because of the excess electron trapping and recombination in the amorphous surroundings, these centers cannot contribute to electron transfer to the surroundings. To further illustrate this aspect, we performed classic photocatalytic decay measurement for the degradation of the dye AO7 (Figure S15) and fluorescence tests for ·OH radical generation (Figure 4 b). In the AO7 tests we observe that either amorphous tubes or tubes with a high-dose implant are considerably less active than pure anatase or low-dose-implanted tubes. In this process the low-dose-implanted tubes do not outperform the anatase tubes—the degradation of AO7 is mainly a valence-band-controlled process.[15,18] However, when using the classic terephthalic acid test for the identification of photo-induced radical species related to conduction-band electron transfer to the electrolyte (Figure 4 b and Supporting Information), we find that the low-dose tubes show a drastically higher electron-transfer rate than anatase tubes or the high-dose-implanted tubes. (Amorphous material shows virtually no activity.)

Overall, we find that low-dose (sufficiently high energy) nitrogen implantation into anatase TiO_2 nanotubes leads to an intrinsic co-catalytic effect that strongly promotes the photocatalytic H_2 evolution performance of TiO_2 nanotube layers without the use of any (noble metal) co-catalyst. This is

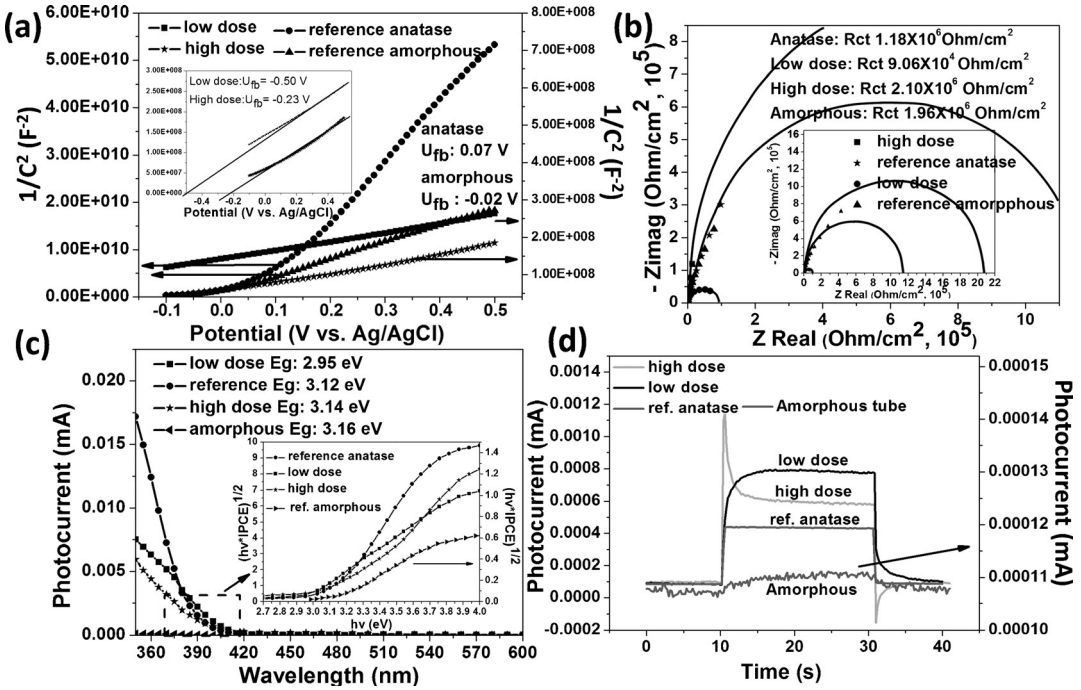

Figure 3. Electrochemical and photoelectrochemical characterization for the N-implanted, reference, and amorphous TiO_2 nanotubes. a) Mott–Schottky plots (inset: enlarged plots for the low- and high-dose N-implanted samples) obtained in 0.1 M Na_2SO_4. b) Nyquist plots from the EIS measurements in 0.1 M Na_2SO_4 at 200 mV (vs. Ag/AgCl). The inset shows the full range Nyquist plot. c) Photocurrent spectra in 0.1 M Na_2SO_4 at 500 mV (vs. Ag/AgCl) (inset: band-gap valuation from the photocurrent spectra). d) Photocurrent transients taken at 405 nm in 0.1 M Na_2SO_4 at 500 mV (vs. Ag/AgCl). All tubes were as shown in Figure S3.

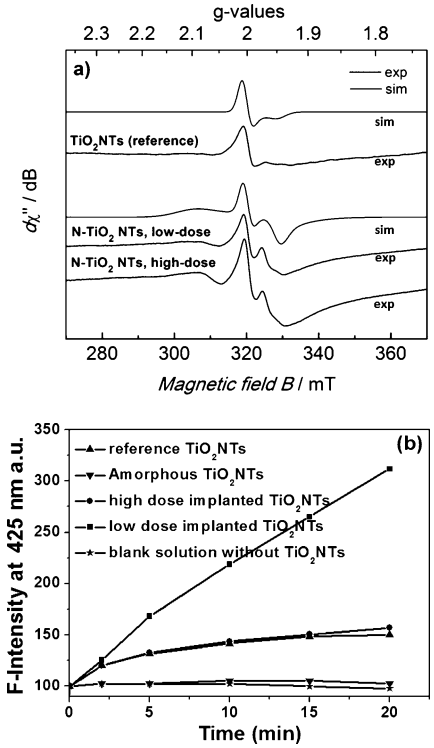

Figure 4. a) CW X-band EPR spectra and simulation of reference (annealed), low-dose nitrogen-implanted and high-dose nitrogen-implanted TiO_2 NTs. b) Test for photocatalytic radical generation based on terephthalic acid;[19] showing $^{\bullet}OH$ radical fluorescence (F) intensity with time for different tubes.

in contrast to high-dose nitrogen implantation that leads to amorphization of the implanted region. Using a sufficiently low dose allows and essentially an intact anatase matrix to be maintained that is dosed with distinct defects and dopants. Electrochemically active states are situated close to the conduction band and are apparent in the capacitance measurements, photocurrent spectra, and photocurrent transients. EPR spectra indicate the presence of a Ti^{3+} configuration that is nitrogen stabilized. A particular advantage of creating these defect centers by N-implantation is that the active centers can be placed as a coherent layer at a subsurface location determined by the selected energy—that is, in vertically aligned TiO_2 nanotubes an active zone (junction) can be embedded in intact nanotubes and a highly synergistic combination of light/electron harvesting and co-catalytic activity can be established.

Acknowledgements

We would like to thank ERC, DFG, the EAM cluster of excellence, as well as the DFG "FunCOS" unit for financial support. We also thank Yuyun Yang for the Raman measurements.

Keywords: H_2 evolution · ion implantation · nitrogen · photocatalysis · TiO_2 nanotubes

How to cite: *Angew. Chem. Int. Ed.* **2016**, *55*, 3763–3767
Angew. Chem. **2016**, *128*, 3827–3831

[1] A. Fujishima, K. Honda, *Nature* **1972**, *238*, 37 – 38.
[2] a) A. Bard, *Science* **1980**, *207*, 139 – 144; b) A. L. Linsebigler, G. Lu, J. T. Yates, *Chem. Rev.* **1995**, *95*, 735 – 758; c) M. R. Hoffmann, S. T. Martin, W. Choi, D. W. Bahneman, *Chem. Rev.* **1995**, *95*, 69 – 96; d) A. Hagfeldt, M. Grätzel, *Chem. Rev.* **1995**, *95*, 49 – 68.
[3] a) K. Lee, A. Mazare, P. Schmuki, *Chem. Rev.* **2014**, *114*, 9385 – 9454; b) P. Roy, S. Berger, P. Schmuki, *Angew. Chem. Int. Ed.* **2011**, *50*, 2904 – 2939; *Angew. Chem.* **2011**, *123*, 2956 – 2995.
[4] a) K. Connelly, A. K. Wahab, H. Idriss, *Mater. Renewable Sustainable Energy* **2012**, *1*, 3; b) M. Ni, M. K. H. Leung, D. Y. C. Leung, K. Sumathy, *Renewable Sustainable Energy Rev.* **2007**, *11*, 401 – 425.
[5] a) J. B. Priebe, J. Radnik, A. J. J. Lennox, M. Pohl, M. Karnahl, D. Hollmann, K. Grabow, U. Bentrup, H. Junge, M. Beller, A. Brückner, *ACS Catal.* **2015**, *5*, 2137 – 2148; b) X. Chen, L. Liu, P. Y. Yu, S. Mao, *Science* **2011**, *331*, 746 – 750; c) G. Wang, H. Wang, Y. Ling, Y. Tang, X. Yang, R. C. Fitzmorris, C. Wang, J. Z. Zhang, Y. Li, *Nano Lett.* **2011**, *11*, 3026 – 3033.
[6] X. Chen, S. S. Mao, *Chem. Rev.* **2007**, *107*, 2891 – 2959.
[7] a) N. Liu, C. Schneider, D. Freitag, M. Hartmann, U. Venkatesan, J. Müller, E. Spiecker, P. Schmuki, *Nano Lett.* **2014**, *14*, 3309 – 3313; b) N. Liu, C. Schneider, D. Freitag, U. Venkatesan, V. R. R. Marthala, M. Hartmann, B. Winter, E. Spiecker, A. Osvet, E. M. Zolnhofer, K. Meyer, T. Nakajima, X. Zhou, P. Schmuki, *Angew. Chem. Int. Ed.* **2014**, *53*, 14201 – 14205; *Angew. Chem.* **2014**, *126*, 14425 – 14429; c) X. Zhou, N. Liu, P. Schmuki, *Electrochem. Commun.* **2014**, *49*, 60 – 64.
[8] a) A. Fujishima, X. Zhang, D. Tryk, *Surf. Sci. Rep.* **2008**, *63*, 515 – 582; b) H. Chen, C. E. Nanayakkara, V. H. Grassian, *Chem. Rev.* **2012**, *112*, 5919 – 5948; c) U. Diebold, *Surf. Sci. Rep.* **2003**, *48*, 53 – 229; d) F. Zuo, L. Wang, T. Wu, Z. Zhang, D. Borchardt, P. Feng, *J. Am. Chem. Soc.* **2010**, *132*, 11856 – 11857; e) T. L. Thompson, J. Yates, *Chem. Rev.* **2006**, *106*, 4428 – 4453; f) H. G. Yang, C. H. Sun, S. Z. Qiao, J. Zou, G. Liu, S. C. Smith, H. M. Cheng, G. Q. Lu, *Nature* **2008**, *453*, 638 – 641; g) J. Dong, R. Ullal, J. Han, S. Wei, J. D. X. Ouyang, W. Gao, *J. Mater. Chem. A* **2015**, *3*, 5285 – 5288.
[9] J. F. Ziegler, J. P. Biersack, U. Littmark, *The Stopping and Range of Ions in Solids*, Pergamon Press, New York, **1985**.
[10] R. Asahi, T. Morikawa, H. Irie, T. Ohwaki, *Chem. Rev.* **2014**, *114*, 9824 – 9852.
[11] a) S. Livraghi, M. C. Paganini, E. Giamello, A. Selloni, C. D. Valentin, G. Pacchioni, *J. Am. Chem. Soc.* **2006**, *128*, 15666 – 15671; b) C. Di Valentin, E. Finazzi, G. Pacchioni, A. Selloni, S. Livraghi, M. C. Paganini, E. Giamello, *Chem. Phys.* **2007**, *339*, 44 – 56.
[12] A. Ghicov, J. M. Macak, H. Tsuchiya, J. Kunze, *Nano. Lett.* **2006**, *6*, 1080 – 1082.
[13] P. Y. Yu, M. Cardona, *Fundamentals of Semiconductors: Physics and Materials Properties*, Springer, Heidelberg, **2010**.
[14] Y. Yan, M. Han, A. Konkin, T. Koppe, D. Wang, T. Andreu, G. Chen, U. Vetter, J. Morantee, P. Schaafa, *J. Mater. Chem. A* **2014**, *2*, 12708 – 12716.
[15] I. Paramasivam, H. Jha, N. Liu, P. Schmuki, *Small* **2012**, *8*, 3073 – 3103.
[16] a) L. Bonneviot, G. Haller, *J. Catal.* **1988**, *113*, 96 – 105; b) A. Brückner, *Chem. Soc. Rev.* **2010**, *39*, 4673 – 4684.
[17] J. M. Coronado, A. Maira, J. C. Conesa, K. Yeung, V. Augugliaro, J. Soria, *Langmuir* **2001**, *17*, 5368 – 5374.
[18] a) H. Gerischer, A. Heller, *J. Phys. Chem.* **1991**, *95*, 5261 – 5267; b) M. Midaka, H. Kubata, M. Grätzel, N. Serpone, E. Pelizzetti, *Nouv. J. Chim.* **1985**, *9*, 67.
[19] K. Ishibashi, A. Fujishima, T. Watanabe, K. Hashimoto, *J. Photochem. Photobiol. A* **2000**, *134*, 139 – 142.

Received: December 13, 2015
Published online: February 15, 2016

